Journal of Biosafety and Biosecurity 5 (2023) 118–132

Contents lists available at ScienceDirect

Journal of Biosafety and Biosecurity

journal homepage: www.keaipublishing.com/en/journals/journal-of-biosafety-and-biosecurity/

Research Article

Comparison of the binding energies of approved mpox drugs and phytochemicals through molecular docking, molecular dynamics simulation, and ADMET studies: An *in silico* approach

Ranjan K. Mohapatra [a,1,*], Ahmed Mahal [b,1], Azaj Ansari [c,1], Manjeet Kumar [c], Jyoti Prakash Guru [d], Ashish K. Sarangi [e], Aly Abdou [f,*], Snehasish Mishra [g], Mohammed Aljeldah [h], Bashayer M. AlShehail [i], Mohammed Alissa [j], Mohammed Garout [k], Ahmed Alsayyah [l], Ahmad A. Alshehri [m], Ahmed Saif [n], Abdulaziz Alqahtani [n], Fahd A. Alshehri [o], Aref A. Alamri [p], Ali A. Rabaan [q,r,s,*]

[a] Department of Chemistry, Government College of Engineering, Keonjhar 758002, Odisha, India
[b] Department of Medical Biochemical Analysis, College of Health Technology, Cihan University—Erbil, Erbil, Kurdistan Region, Iraq
[c] Department of Chemistry, Central University of Haryana, Mahendergarh, Haryana 123031, India
[d] Department of Pharmaceutics, School of Pharmacy, Centurion University of Technology and Management, Balangir, Odisha 767001, India
[e] Department of Chemistry, School of Applied Sciences, Centurion University of Technology and Management, Balangir, Odisha 767001, India
[f] Chemistry Department, Faculty of Science, Sohag University, Sohag 82524, Egypt
[g] School of Biotechnology, Campus-11, KIIT Deemed-to-be-University, Bhubaneswar 751 024, Odisha, India
[h] Department of Clinical Laboratory Sciences, College of Applied Medical Sciences, University of Hafr Al Batin, Hafr Al Batin 39831, Saudi Arabia
[i] Pharmacy Practice Department, College of Clinical Pharmacy, Imam Abdulrahman Bin Faisal University, Dammam 31441, Saudi Arabia
[j] Department of Medical Laboratory Sciences, College of Applied Medical Sciences, Prince Sattam bin Abdulaziz University, Al-Kharj 11942, Saudi Arabia
[k] Department of Community Medicine and Health Care for Pilgrims, Faculty of Medicine, Umm Al-Qura University, Makkah 21955, Saudi Arabia
[l] Department of Pathology, College of Medicine, Imam Abdulrahman Bin Faisal University, Dammam 31441, Saudi Arabia
[m] Department of Clinical Laboratory Sciences, College of Applied Medical Sciences, Najran University, Najran 61441, Saudi Arabia
[n] Department of Clinical Laboratory Sciences, College of Applied Medical Sciences, King Khalid University, Abha 62223, Saudi Arabia
[o] Nursing Administration, East Jeddah Hospital, Jeddah 22253, Saudi Arabia
[p] Molecular Microbiology and Cytogenetics Department, Riyadh Regional Laboratory, Riyadh 11425, Saudi Arabia
[q] Molecular Diagnostic Laboratory, Johns Hopkins Aramco Healthcare, Dhahran 31311, Saudi Arabia
[r] College of Medicine, Alfaisal University, Riyadh 11533, Saudi Arabia
[s] Department of Public Health and Nutrition, The University of Haripur, Haripur 22610, Pakistan

ARTICLE INFO

Article history:
Received 7 July 2023
Received in revised form 25 August 2023
Accepted 6 September 2023

Keywords:
ADMET
DFT
MD simulation
Molecular docking
Mpox
QSAR

ABSTRACT

The mpox (previously monkeypox) outbreak in more than 100 non-endemic countries in 2022 posed a serious global health concern. Mpox is emerging as a global public health threat from a seemingly neglected disease. A42R profilin-like protein from mpox virus (PDB ID: 4QWO) could be a preferred target lead. The binding affinity of commonly used drugs/mAbs (tecovirimat, brincidofovir, cidofovir) for A42R profilin-like protein was examined *in silico* through molecular docking. Further, the results were compared with those of the phytochemicals curcumin, rutin, and theaflavin. Tecovirimat (−7.31 kcal/mol, IC_{50} = 4.39 μM) and theaflavin (−6.99 kcal/mol, IC_{50} = 7.54 μM) had the highest affinities. Molecular dynamics simulation of the theaflavin–4QWO complex was performed to ascertain the stability of ligand–protein interactions in natural charge, molecular electrostatic potential, and frontier molecular orbital analyses. The predicted QSAR and pharmacokinetic properties of all compounds were evaluated to find a suitable candidate for designing and developing new drugs. The evaluated log P values for brincidofovir and tecovirimat were higher than those of the other drugs in the QSAR study. Theaflavin had an impressive log P of 4.77, which hints at its high biological activity. The findings recommend further *in vitro* experimental validation to develop potential low-cost mpox therapies.

1. Introduction

Mpox (formerly monkeypox) was once endemic to the African continent. Cases rose in more than 100 non-endemic nations in 2022, posing global public health challenges.[1] As a result, the

* Corresponding authors at: Government College of Engineering, Keonjhar 758 002, Odisha, India (R. K. Mohapatra) Johns Hopkins Aramco Healthcare, Dhahran 31311, Saudi Arabia (A.A. Rabaan) Sohag University, Sohag 82524, Egypt (A. Abdou).
E-mail addresses: ranjank_mohapatra@yahoo.com (R.K. Mohapatra), aly_abdou@science.sohag.edu.eg (A. Abdou), arabaan@gmail.com (A.A. Rabaan).
[1] These authors contributed equally, and they are considered co-first authors.

https://doi.org/10.1016/j.jobb.2023.09.001
2588-9338/

World Health Organization (WHO) included it under the category 'public health emergency of international concern' (https://www.who.int/europe/news/item/23-07-2022-who-director-general-declares-the-ongoing-monkeypox-outbreak-a-public-health-event-of-international-concernb) on July 23, 2022. Mpox spreads mainly during close contact with the skin, face, and/or mouth of infected individuals.[2] Human-to-human transmission occurs via the body fluids (respiratory secretions, saliva from coughing, and droplets), skin lesions/contaminated clothing, or bedding of mpox-infected individuals.[3,4] The mpox outbreak in 2022 primarily affected specific sexually active communities such as men who have sex with men, bisexual people, and transgender individuals,[5] although other groups, such as women and non-binary individuals, also contracted the virus.[6,7] Mpox rashes develop in unexpected and hard-to-notice areas such as the anus, genitals including the vagina, mouth, and throat.[8]

Although mpox is generally self-limiting, it could be severe in new-borns, young children, pregnant women, and immunosuppressed individuals based on their health conditions and the nature of their complications.[8] The effect can worsen with underlying immunodeficiency. Complications can also include secondary infections, sepsis, bronchopneumonia, encephalitis, and vision loss. Mpox is an enveloped double-stranded DNA virus belonging to the Poxviridae family (similar as the smallpox virus) and *Orthopoxvirus* genus. This zoonotic virus consists of Central African and West African clades,[7] and the latter clade (consisting of subclades a and b) reportedly dominated the 2022 outbreak. The research gap in understanding the replication process of mpox during infection is immense, and the origin of the 2022 mpox outbreak remains mysterious.

Supportive care, symptomatic treatment, and bacterial superinfection management for skin lesions and eye infections and complications are valuable treatment options for mpox.[9] Primarily developed against smallpox, the antiviral tecovirimat is currently used against mpox, although it is not yet widely available.[10] Critical cases can be treated with vaccinia immunoglobulin intravenous, cidofovir, and brincidofovir.[2,9–12] No vaccine provides 100% protection, and the effectiveness of currently available mpox vaccines such as JYNNEOS™ and ACAM2000® appears dubious. In view of viral mutations, breakthrough infections, and the side effects of vaccines, a safer and efficacious next-generation vaccine that remains effective against mutants has been recommended.[13] The present work examined the binding affinities of tecovirimat, brincidofovir, and cidofovir for A42R profilin-like protein in an *in silico* through molecular docking study. The results were compared with those of curcumin, rutin, and theaflavin via *in silico* drug design. ADMET data analyses were used to assess the drug-likeness of the test compounds.

2. Materials and methods

2.1. Quantum chemical studies

An *ab initio* estimation of the properties of the test molecules was performed using Gaussian 09 W software.[14,15] To assess electronic structure characteristics, the Becke, three-parameter, Lee–Yang–Parr (B3LYP) hybrid functional[16,17] with a 6–311++G (d,p) basis set[18,19] was employed, and to optimise the molecular structures of test molecules, frontier molecular orbitals (FMOs) and molecular electrostatic potential (MEP) were used. The highest (E_{HOMO}) and lowest (E_{LUMO}) energies of the unoccupied molecular orbital, gap energy (ΔE_{gap}), dipole moment (μ), electron affinity (A), ionisation potential (I), electronegativity (χ), electrophilicity index (ω), electronic chemical potential (μ), and global hardness (η), and softness (S) were measured, and the electronic features were analysed following the available literature.

2.2. Molecular docking study

The affinity of the test compounds for A42R profilin-like protein (PDB ID: 4QWO) was calculated by receptor-oriented molecular docking using AutoDock Vina (open-source) software.[20,21] The 3D protein structure was taken from the PDB database (https://www.rcsb.org/structure/4qwo).[22] Recently, the X-ray crystal structure (1.52 Å resolution) of the mpox A42R profilin-like protein was reported.[23] The structure was generated using the Chimera suite[24] by adding and optimising hydrogen atoms and removing any atomic/steric clashes. Ligands were obtained from PubChem in the.sdf format and saved by converting them into the PDBQT format. The Kollman charge, fragmental volume and attribute, solvation parameter, and polar hydrogen were adjusted using AutoDock tools. The AutoGrid engine was used to make a grid box around the protein-binding site. The ligand with best possible binding energy and lowest docking score was further analysed. The 2D and 3D interactions were visualised using Discovery Studio 3.5.

2.3. IC_{50} prediction

IC_{50}, which represents the half-maximal inhibitory concentration, measures a ligand's specific potency in the inhibition of biological function. AutoDock v4.2 was used to determine the predicted IC_{50} for each test ligand.[25] For the best docking conformer, the Lamarckian genetic algorithm (LGA) with default ×, y, and z atomic salvation parameters of 126 Å was chosen.[26] LGA cluster analysis was used to collect binding energies with IC_{50} values for various docking forms. With respect to the IC_{50}, the lowest binding energy of the docking results was considered. Calculations were repeated three times to confirm the confluence of the results.

2.4. Molecular dynamics (MD) simulation

MD simulation was performed to assess the stability of protein–ligand (P-L) complex leads. The best-scored conformations of receptor–ligand systems were determined using the Desmond v3.6 package (DE Shaw Research, New York, New York, USA). OPLS_2005 force field MD simulation was performed for 100 ns to analyse the theaflavin–4QWO complex.[27] The system builder tool of Desmond was used to fix the ×, y, and z dimensions of the cubical water box (TIP3P water model) with a buffer space of 10 Å[28] and box volume of 478,000 Å^3. As required for each system, Na^+ and Cl^- counterions were added. MD simulation was conducted with a temperature of 300 K, pressure of 1 atm, and thermostat relaxation time of 200 ps.[29] Temperature and pressure were regulated using the Nose–Hoover chain thermostat and Martyna–Tobias–Klein barostat methods.[30,31] As the system relaxed, a 100 ns run under NPT ensemble was executed.

3. Results and discussion

3.1. FMO analysis and chemical reactivity

The optimised structures of the test molecules are presented in Fig. 1. FMO analysis provides researchers with data on chemical reactivity. FMOs are the related energies of a compound's E_{LUMO} and E_{HOMO}. HOMO reflects electron-donating ability, and LUMO reflects electron-accepting ability.

The E_{LUMO} values of brincidofovir, cidofovir, rutin, tecovirimat, and theaflavin were −6.14, −6.80, −5.65, −7.16, and −5.65 eV,

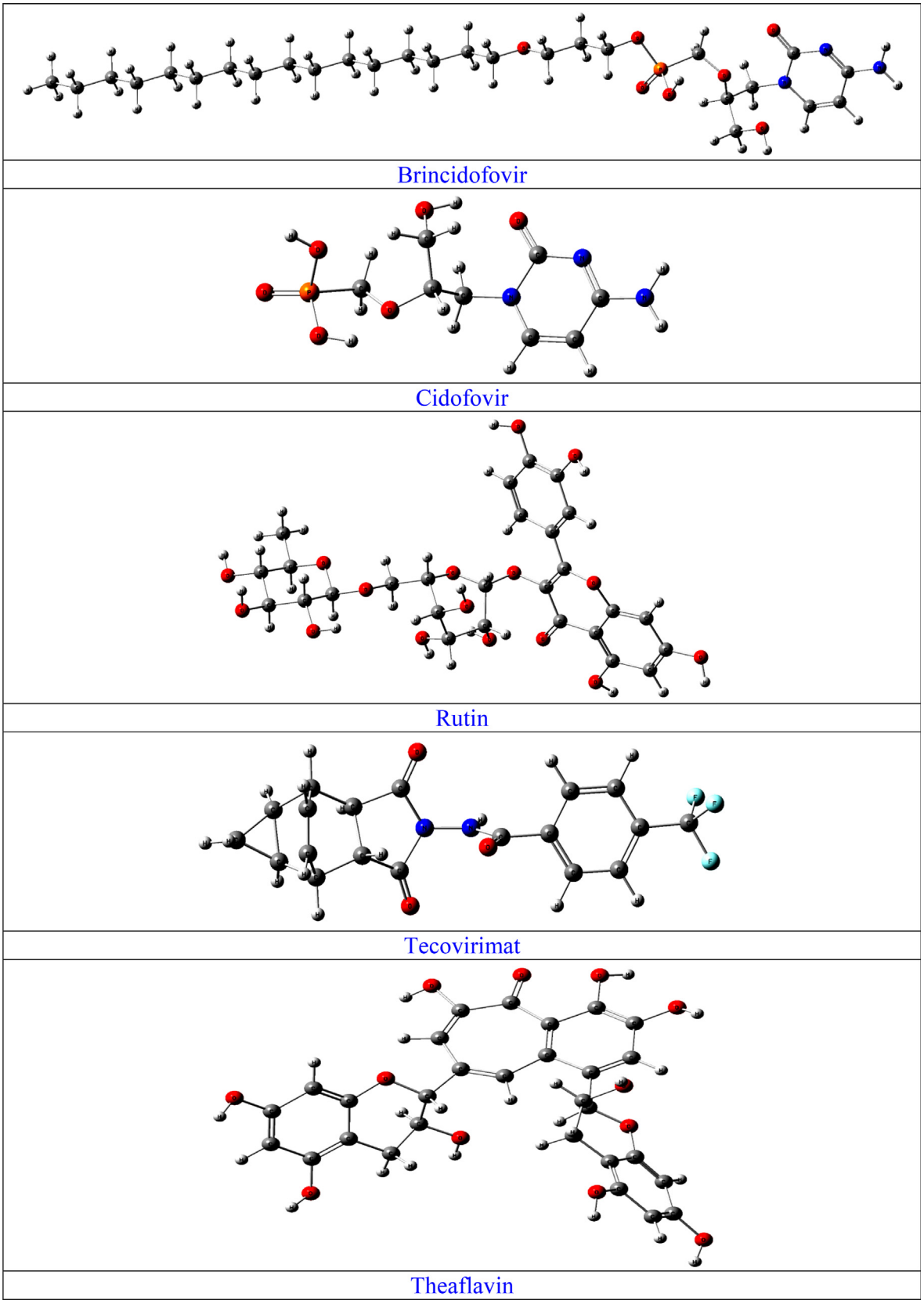

Fig. 1. The obtained optimised structures of brincidofovir, cidofovir, rutin, tecovirimat, and theaflavin with atom numbering in the gaseous phase using B3LYP/6–311++G(d,p).

respectively, whereas the E_{HOMO} values of these compounds were −1.00, −1.74, −2.06, −1.56, and −1.76 eV, respectively. The chemical stability of a molecule is described by ΔE_{gap}.[32] The ΔE_{gap} values of brincidofovir, cidofovir, rutin, tecovirimat, and theaflavin were 5.14, 5.06, 3.59, 5.59, and 3.88 eV, respectively. The structural reactivity of a test molecule is demonstrated by a low ΔE_{gap}.[33] A mole-

cule is a soft molecule when its ΔE_{gap} is small, indicating that it is highly polarisable, which is associated with low kinetic stability and high chemical reactivity.

The HOMO and LUMO maps incorporated into the structures of brincidofovir, cidofovir, rutin, tecovirimat, and theaflavin are depicted in Fig. 2. The negative and positive phases of the molecu-

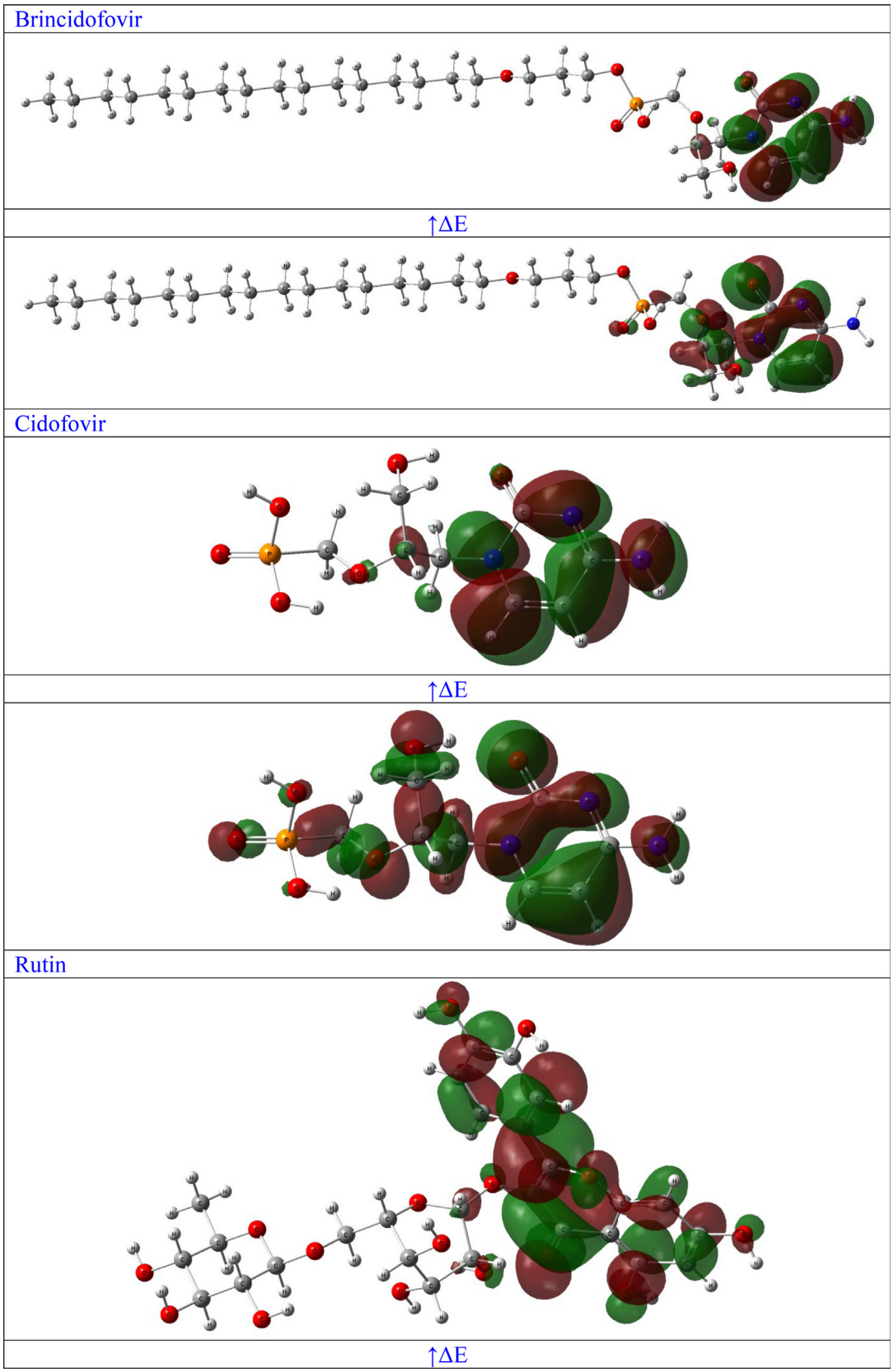

Fig. 2. FMOs of brincidofovir, cidofovir, rutin, tecovirimat, and theaflavin in the gaseous phase using B3LYP/6–311++G(d,p).

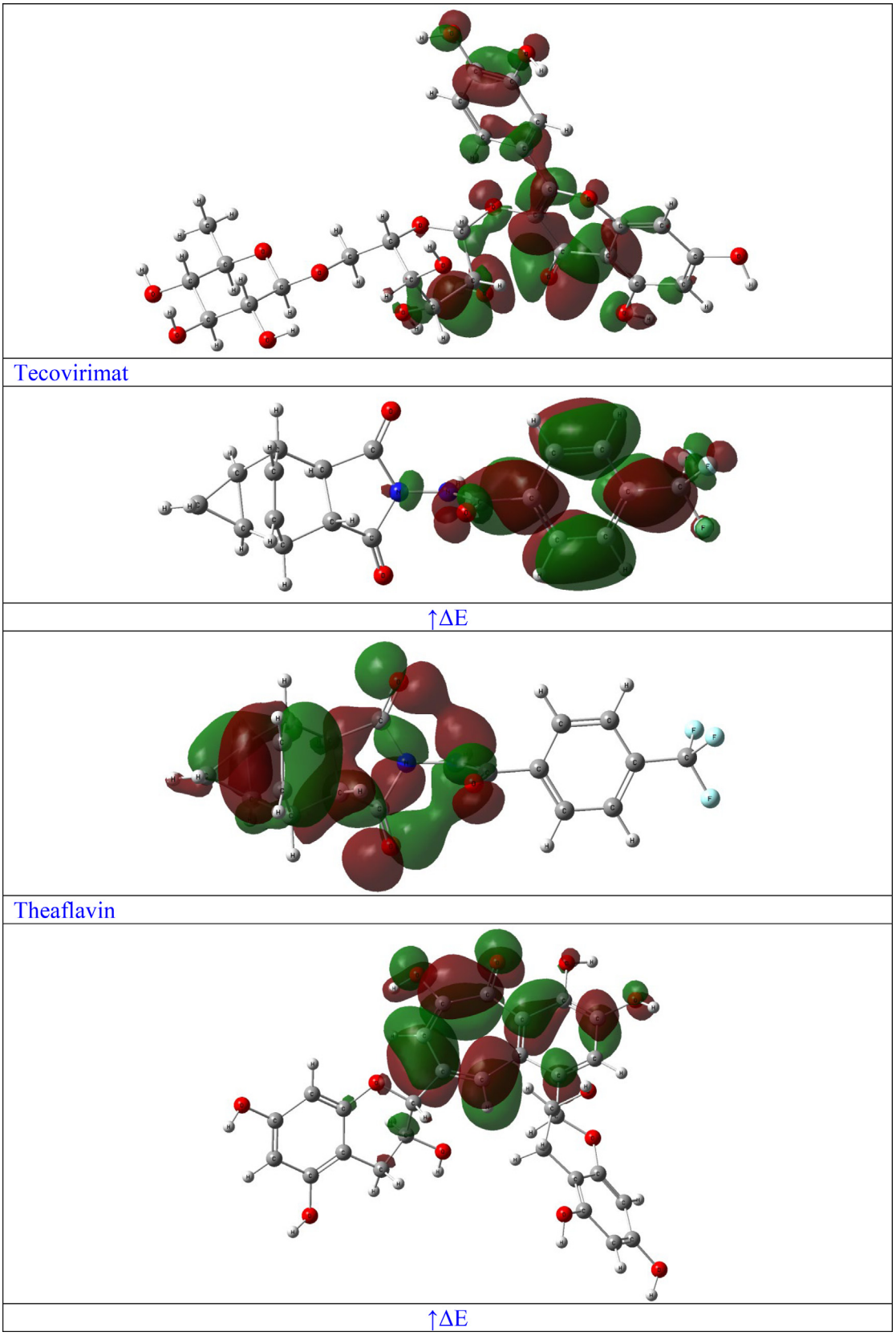

Fig. 2 (*continued*)

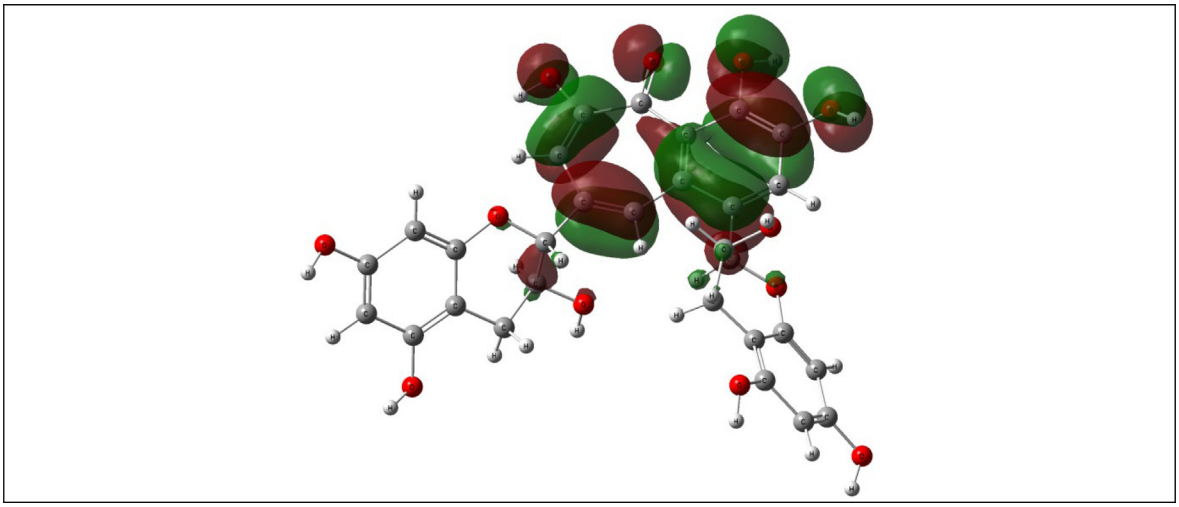

Fig. 2 (*continued*)

Table 1
Calculated chemical parameters.

	E_{Total}	μ	E_{HOMO}	E_{LUMO}	ΔE	I	A	χ	CP	η	σ	ω
Brincidofovir	−56949.56	6.38	−6.14	−1.00	5.14	6.14	1.00	3.57	−3.57	2.57	0.19	2.48
Cidofovir	−34573.33	9.94	−6.80	−1.74	5.06	6.80	1.74	4.27	−4.27	2.53	0.20	3.60
Rutin	−61246.10	2.05	−5.65	−2.06	3.59	5.65	2.06	3.86	−3.86	1.80	0.28	4.14
Tecovirimat	−37225.19	5.06	−7.16	−1.56	5.59	7.16	1.56	4.36	−4.36	2.80	0.18	3.40
Theaflavin	−55034.46	12.61	−5.65	−1.76	3.88	5.65	1.76	3.71	−3.71	1.94	0.26	3.54

lar orbital wave function distributions are represented in green and red, respectively. The images (Fig. 2) indicate that LUMOs and HOMOs are mostly concentrated across the entire molecule structure of each compound.

The relationship between structural stability and global chemical reactivity relies on the understanding of global reactivity parameters. The calculated E_{HOMO}, E_{LUMO}, ΔE_{gap}, I, A, total energy of the optimised molecular structure (E_{Total}), and global reactivity properties such as χ, μ, ω, η, and S of brincidofovir, cidofovir, rutin, tecovirimat, and theaflavin in the gaseous phase are presented in Table 1. The optimised geometries of brincidofovir, cidofovir, rutin, tecovirimat, and theaflavin, which had E_{Total} values of −56,949.56, −33,573.33, −61,246.10, −37,225.19, and −55034.46 eV, respectively (Table 1), indicated high stability.

The μ values of brincidofovir, cidofovir, rutin, tecovirimat, and theaflavin in the gaseous phase produced using the DFT technique were 6.38, 9.94, 2.05, 5.06, and 12.61 Debye, respectively. They exhibited low I values as follows: brincidofovir, 6.14 eV; cidofovir, 6.80 eV; rutin, 5.65 eV; tecovirimat, 7.16 eV; and theaflavin, 5.65 eV. These values indicate good electron-donating properties. The global values of η and S were estimated as follows: brincidofovir, 2.57 and 0.19 eV, respectively; cidofovir, 2.53 and 0.20 eV, respectively; rutin, 1.80 and 0.28 eV, respectively; tecovirimat, 2.80 and 0.18 eV, respectively; and theaflavin, 1.94 and 0.26 eV, respectively. A useful interpretation of the values is as intramolecular charge transfer indicator. Low η and high S values indicate that a test structure is a soft molecule.

The ω values of brincidofovir, cidofovir, rutin, tecovirimat, and theaflavin were 2.48, 3.60, 4.14, 3.40, and 3.54 eV, respectively. According to Domingo et al., the compounds were all categorised as "high electrophiles" (>1.50 eV).[34] The ability of an atom or set of atoms to draw electrons is quantified by χ. According to our calculations, the χ values of brincidofovir, cidofovir, rutin, tecovirimat, and theaflavin were 3.57, 4.27, 3.86, 4.36, and 3.71 eV, respectively, whereas the μ values were − 3.57, −4.27, −3.86, −4.36, and −3.71 eV, respectively (Table 1).

3.2. MEP

MEP is valuable for illustrating molecular electronic density, and it is used to identify both positive and negative surface electrostatic potentials with coloured dots.[35] Red, orange, or yellow 'negative' sites (high electron density) represent electrophilic assault; green 'positive' sites (low electron density) reflect nucleophilic attack; and blue 'positive' sites (high electron density) represent neutral regions. The MEPs of brincidofovir, cidofovir, rutin, tecovirimat, and theaflavin (Fig. 3) were calculated using B3LYP/6–311++G(d,p)(Gas).

The negative areas of brincidofovir, cidofovir, rutin, tecovirimat, and theaflavin were located around O_2 atoms (Fig. 3). The H atom linked to N was the centre of the positive areas, making it vulnerable to nucleophilic assault. The faint blue areas represented weak interaction locations, and the green regions presented neutral areas with no potential.

3.3. Natural charge analyses

Atomic charges in molecules are significant because they represent the physicochemical properties of molecules such as the electronic structure, dipole moment, vibrational spectra, and polarisability, and others.[36] The gaseous-phase atomic charges of brincidofovir, cidofovir, rutin, tecovirimat, and theaflavin were analysed by NBO (explaining intramolecular charge transfer among the bonding and antibonding orbitals) using B3LYP/6–311++G(d,p) (Fig. S1).

The electronegativity equalisation and charge transfer in the chemical reactivity of the test molecules were analysed by NBO. This revealed that the carbon atoms in brincidofovir, cidofovir, rutin, tecovirimat, and theaflavin contained both positive and negative charges. Positive atoms were coupled to electron-

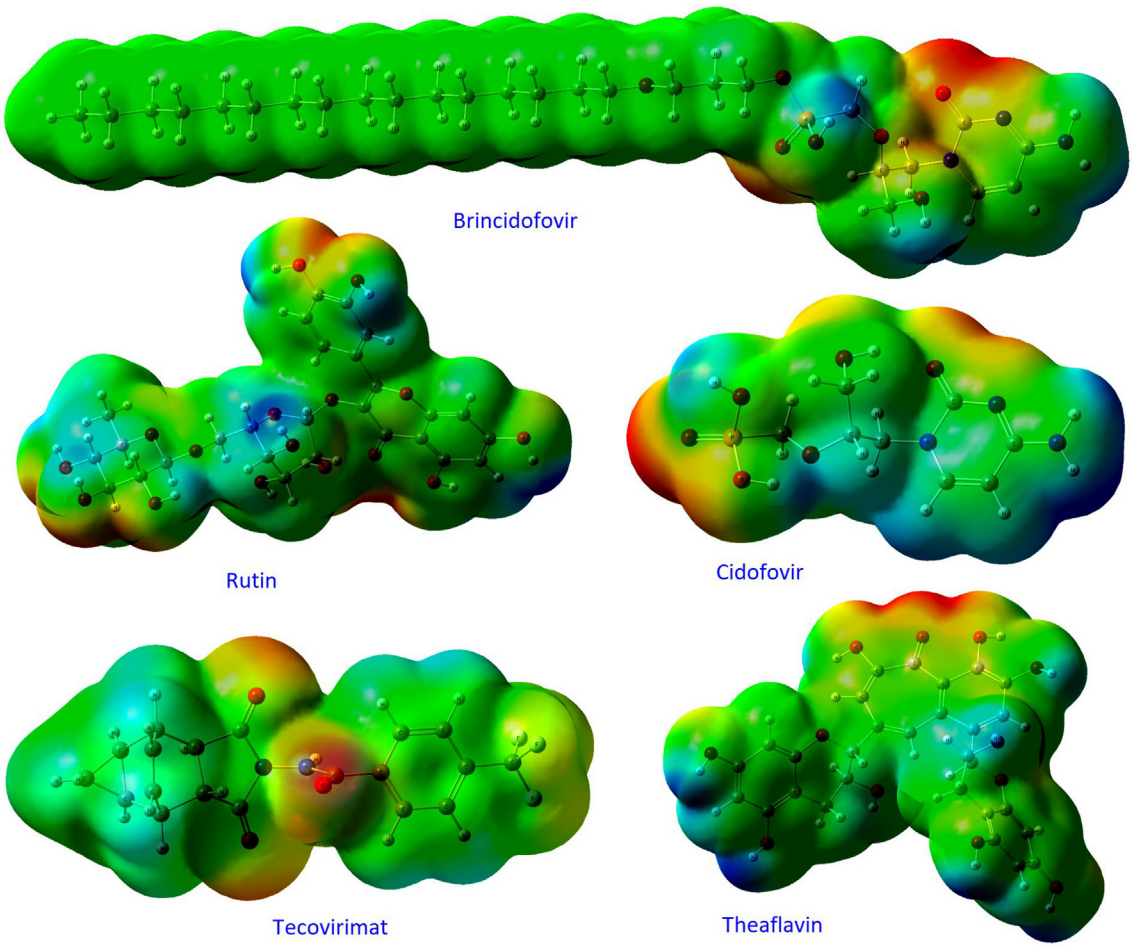

Fig. 3. Computed gaseous-phase MEP maps of the test compounds using B3LYP/6–311++G(d,p).

withdrawing oxygen and nitrogen atoms (Fig. S1) at P1, C36, C38, C30, and C35 in brincidofovir; P1, C16, C18, C11, and C15 in cidofovir; C31, C22, C25, and C35 in rutin; C27, C19, C18, and C20 in tecovirimat; and C33, C41, C39, and C25 in theaflavin. All hydrogen atoms were positively charged. O50, O40, O140, N8, and O60 were electron-withdrawing atoms, meaning that H86, H29, H71, H38, and H60 (hydrogen) had major positive charges compared with other hydrogen atoms.

Other atoms such as carbon atoms (brincidofovir: C17, C21, C23, C22, C24, C29; cidofovir: C11, C15, C13, C12, C17, C14; rutin: C20, C26, C33, C38, C37, C42, C32; tecovirimat: C16, C9, C10, C13, C12, C14, C15; and theaflavin: C29, C37, C36, C40, C38, C18, C21) had negative charges. Additionally, P1 in brincidofovir (2.178610), P1 in cidofovir (2.23806), C31 in rutin (0.45742), C27 in tecovirimat (1.10624), and C33 in theaflavin (0.45937) had the greatest positive charges, as they were connected to withdrawing oxygen atoms (O50 and O70 in brincidofovir; O50 and O40 in cidofovir; O120 in rutin; F1, F2, and F3 in tecovirimat; and O100 in theaflavin) opposite other carbon atoms. As was deciphered, all hydrogen atoms were positively charged. The most negatively charged atoms were C29 in brincidofovir (−0.41447), C14 in cidofovir (−0.38262), C39 in rutin (−0.34635), C15 in tecovirimat (−0.2992), and C21 in theaflavin (−0.41332).

3.1. Molecular docking analyses

Molecular docking is an efficient tool in structure-based drug discovery.[37] The binding interactions between the target protein (PDB ID: 4QWO) and the test ligands (brincidofovir, cidofovir, tecovirimat, curcumin, rutin, and theaflavin) were predicted. All ligands interacted with the A42R profilin-like protein of mpox in the binding pocket cavity, with all compounds binding to the amino acids HIS5, HIS55, PRO36, ASN30, ASN37, ALA33, ALA41, and ILE8 (Fig. 4. and Fig. S2). The best-pose docking scores (binding free energy) were observed in the range of − 7.31 (tecovirimat) to − 1.5 (brincidofovir). Theaflavin also had an attractive binding energy of − 6.99. The binding energy and predicted IC_{50} values for all ligands are listed in Table 2.

3.2. MD simulation

With their high binding energies and low predicted IC_{50} values, tecovirimat and theaflavin displayed significant interactions with the protein target 4QWO. Theaflavin was subjected to MD simulation as the lead compound. For insights into the stability of the theaflavin–A42R profilin-like protein complex, the MD simulation was performed for 100 ns. The overall stability was further investigated by analysing the root mean square deviation (RMSD) and root mean square fluctuation (RMSF; Figs. S3–S5).

3.2.1. Protein RMSD

The MD simulation was performed to examine the P-L interactions using Schrödinger's Desmond package.[38–41] The 100 ns theaflavin–4QWO complex simulation was performed to calculate the RMSD and RMSF (Figs. 5 and 6). The overall RMSD of theaflavin reached a maximum of 2.0 Å, suggesting that the complex was stable (a low RMSD indicates greater stability). After initial fluctuation up to nearly 5 ns, RMSD slowly reached equilibrium. For the

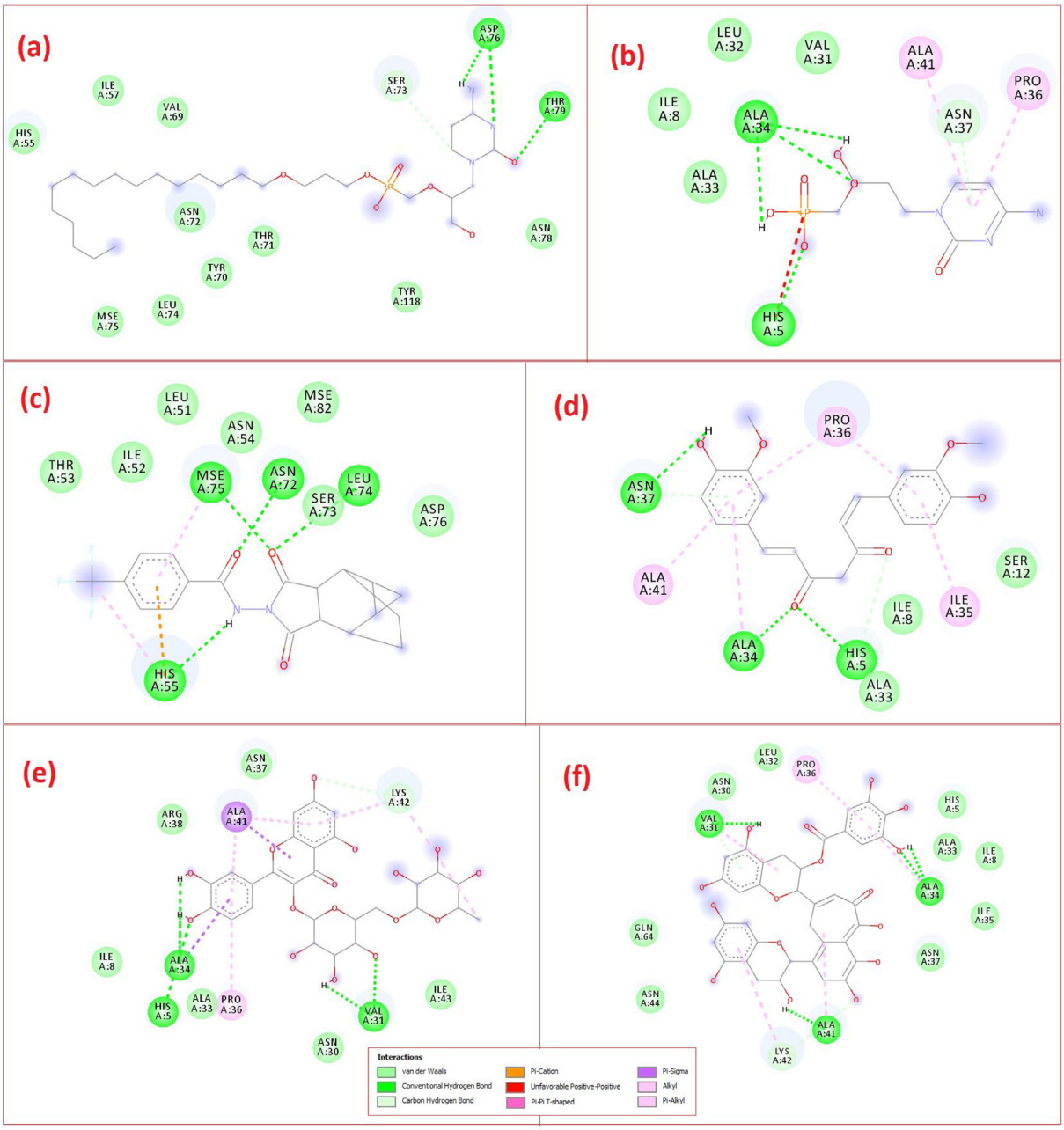

Fig. 4. 2D interactions of the test ligands with A42R profilin-like protein (PDB ID: 4QWO).

Table 2
Docking of the test ligands with A42R profilin-like protein (PDB ID: 4QWO).

Sl. No.	Ligand	Binding energy (kcal/mol)	IC_{50} value
1	Brincidofovir	−1.5	79.59 mM
2	Cidofovir	−3.5	2.70 mM
3	Tecovirimat	−7.31	4.39 uM
4	Curcumin	−5.03	204.76 uM
5	Rutin	−3.91	1.36 mM
6	Theaflavin	−6.99	7.54 uM

The predicted IC_{50} values for theaflavin and tecovirimat were 7.54 and 4.39 μM, respectively. Considering the binding energy, predicted IC_{50} values, and ADMET properties, tecovirimat and theaflavin were selected as lead compounds, and theaflavin was further analysed.

theaflavin–4QWO complex, the RMSD was 1.7 Å at equilibrium. RMSF maximally fluctuated at 1.6 Å initially and remained lower throughout the simulation (Fig. 6). RMSF helps distinguish the changes along the protein chain. The interactions of the amino acid residues of the protein with the ligand are coloured green in Fig. 6 (vertical bars), and these interactions were further considered for P-L contact analyses. The 'fit on protein' trend (brown line) and 'ligand' trend (pink line) of the RMSF are presented in Fig. S6.

3.2.2. Ligand properties

The RMSD, radius of gyration (rGyr), molecular surface area (MolSA), solvent accessible surface area (SASA), and polar surface area (PSA) of the ligand were analysed. With fluctuation, the RMSD of the ligand started at 0.6 Å, gradually reaching equilibrium around 1.2 Å (Fig. 7). The rGyr (protein structure compactness) of the ligand started at 4.75 Å, gradually reaching equilibrium around 4.85 Å (Fig. 7). Strong intramolecular H-bond interactions suggested strong inhibition capacity. The ligand exhibited a MolSA

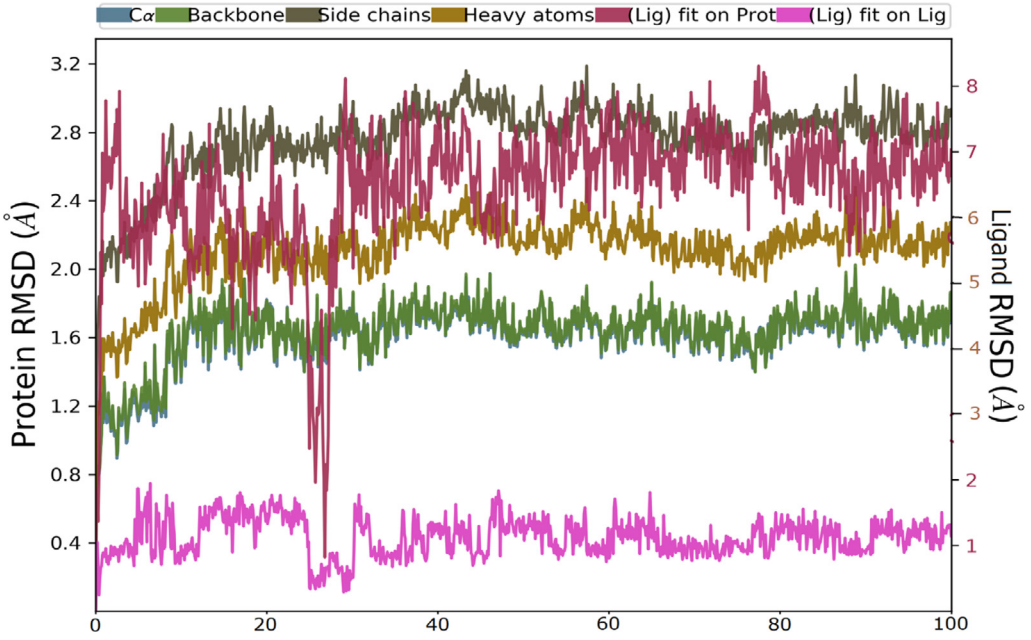

Fig. 5. Protein–ligand RMSD trajectory.

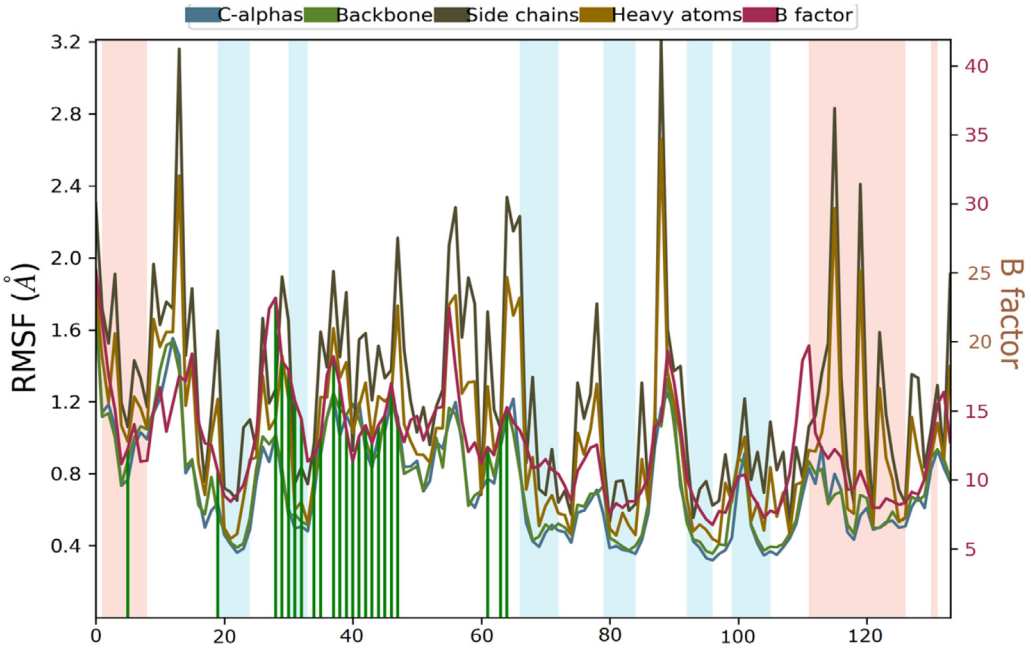

Fig. 6. Protein–ligand RMSF trajectory.

of 420–450 Å^2 with equilibrium at 450 Å^2. The SASA of the ligand started at 390 Å^2, covered a range of 300–480 Å^2, and then gradually approached equilibrium around 360 Å^2. PSA remained constant throughout the simulation. It started from 420 Å^2 and ended at 450 Å^2 at equilibrium. The ligand properties remained constant throughout the simulation with minimal fluctuation in the initial stage and gradually approached equilibrium. The results corroborated the stability of the ligand during interaction with the protein active site.

3.2.3. P-L contacts

P-L interactions are usually one of four types: ionic, hydrophobic, hydrogen bonding, and water bridges. Hydrogen bonding is crucial in drug design and development. Contact histograms (Fig. 8) confirmed the stability of the theaflavin–4QWO complex via P-L contacts.[39,40] The histograms for 4QWO exhibited active-site amino acids (ASN30, VAL31, LEU32, ALA34, ILE35, ASN37, ARG38, THR39, LYS42, ASN44, GLU47, GLN64) interacting via H-bonds with the ligand (Fig. 8 and Figs. S7–S8). VAL31, ALA34, ASN37, ALA41, LYS42, and PRO45 of 4QWO were particularly involved in hydrophobic interactions (Fig. 8; Table S1). The ligand also exhibited ionic interactions with ASN37 and LYS42 at the active site. The 4QWO residues HIS5, LYS29, ASN30, VAL31, LEU32, ALA34, ILE35, ASN37, ARG38, PHE40, ALA41, LYS42, ILE43, ASN44, GLU47, LEU61, GLY63, and GLN64 mainly interacted with the ligand via water bridges. The number of contacts across the tra-

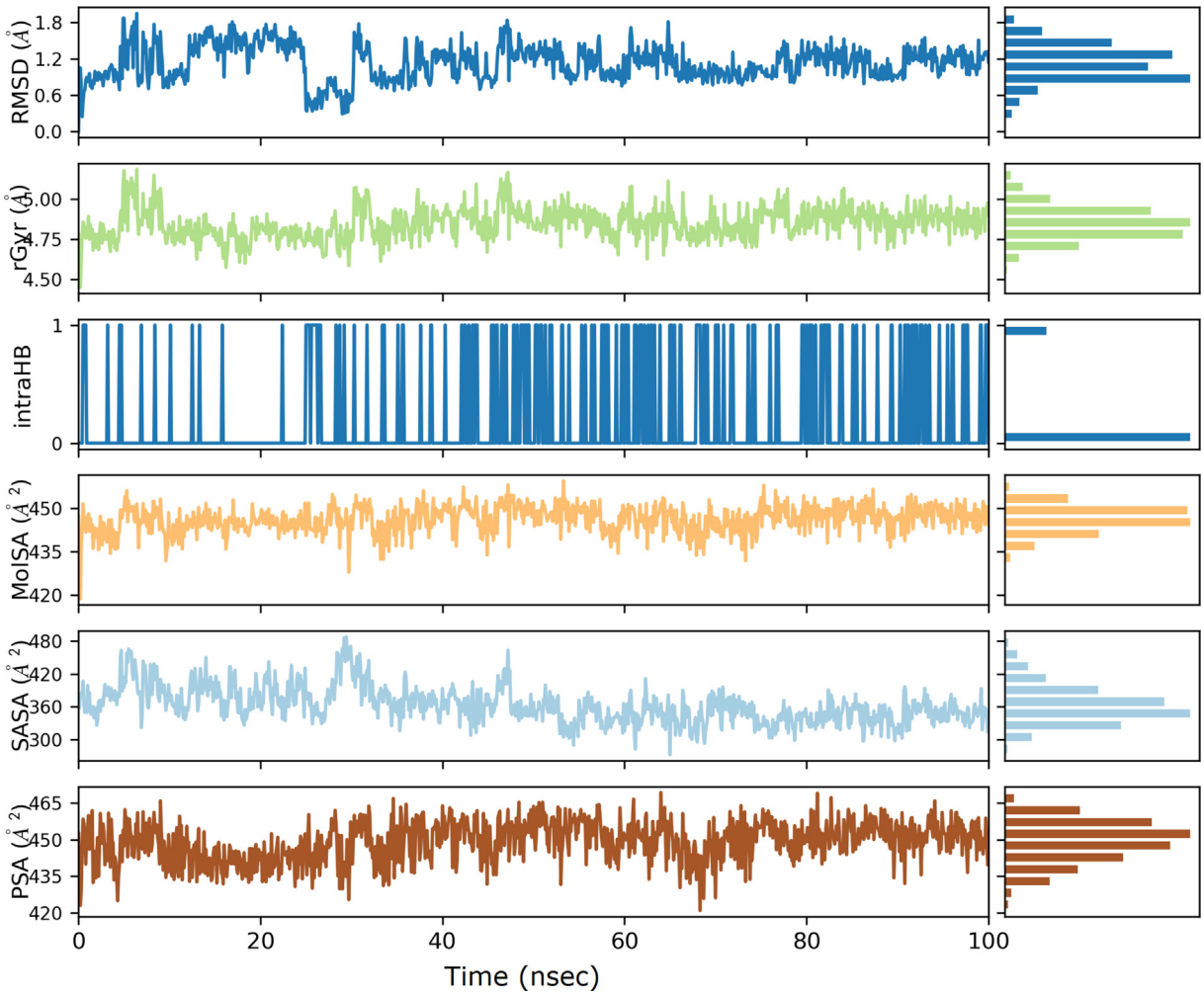

Fig. 7. Ligand property trajectory of the theaflavin–4QWO complex.

jectory varied between 0 and 15. Amino acid contribution was analysed from the P-L binding interaction in each trajectory frame. The theaflavin–4QWO complex had thick bands for LYS29, ASN30, VAL31, ASN37, ARG38, LYS42, PRO45, and GLN64, suggesting that the cited amino acids have more interactions with the ligand in all possible orientations (Fig. 9).

3.2.4. Secondary structure analysis

The secondary structure of a protein is better characterised by α-helix (red) and β-strand (blue) structures (Fig. S9). The secondary structure region covered 46.44% of the entire simulation. The upper half of the plot presents the SSE distribution by residue index in the protein structure, and bottom half summarises the SSE composition for each trajectory frame during simulation.

3.2.5. Torsional analysis

The 2D depiction of theaflavin with colour-coded rotatable bonds (RBs) is schematically presented in Fig. S10 with conformational evolution from 0 to 100 ns for each RB across the simulation trajectory. The rotatable torsional bond was supported by a radial plot with the same colour bar plots. The radial plot explicated torsion angle conformation during simulation. Simulation initiated from the centre of the radial plot oriented to the outside as time progressed. During trajectory-establishing simulation, the torsional conformation of each rotatable bond in theaflavin was computed, and the data of the conformational evolution of each ligand were provided (Fig. S10). The dartboard plots on the left reveal the angle of each bond at a given time during simulation. The radial was central, and the time evolution was outwards. The histograms on the right present the probability of the torsions as a function of the angle. The angular coordinate indicates the torsional angle, and the radial coordinate represents the rotatable bond.[42] The compound has few RBs contributing to its stability.

4. ADMET properties

The pharmacokinetic significance, utility index, and accuracy rate of the model were determined using the ADMET model. A web server (https://biosig.lab.uq.edu.au/pkcsm/) was used to calculate the ADMET variables of the ligand, as it has proven useful for designing target-specific potential leads for small drugs.[43] For drug development, it is essential to predict the effects of a compound on the body, such as the amount absorbed in the gastrointestinal tract when taken orally and its ultimate fate. Poor absorption would affect the distribution and metabolism of a drug and potentially result in neurotoxicity and nephrotoxicity. Further, therapeutic variables such as the water solubility, permeability, volume distribution, unbound fraction, BBB permeability, CNS permeability, total clearance, and toxicity of a test molecule can be predicted using ADMET data (Table 3). The Caco-2 human intestinal mucosa cell line is frequently used as an *in vitro* model to predict the absorption of orally administered drug. Intestinal

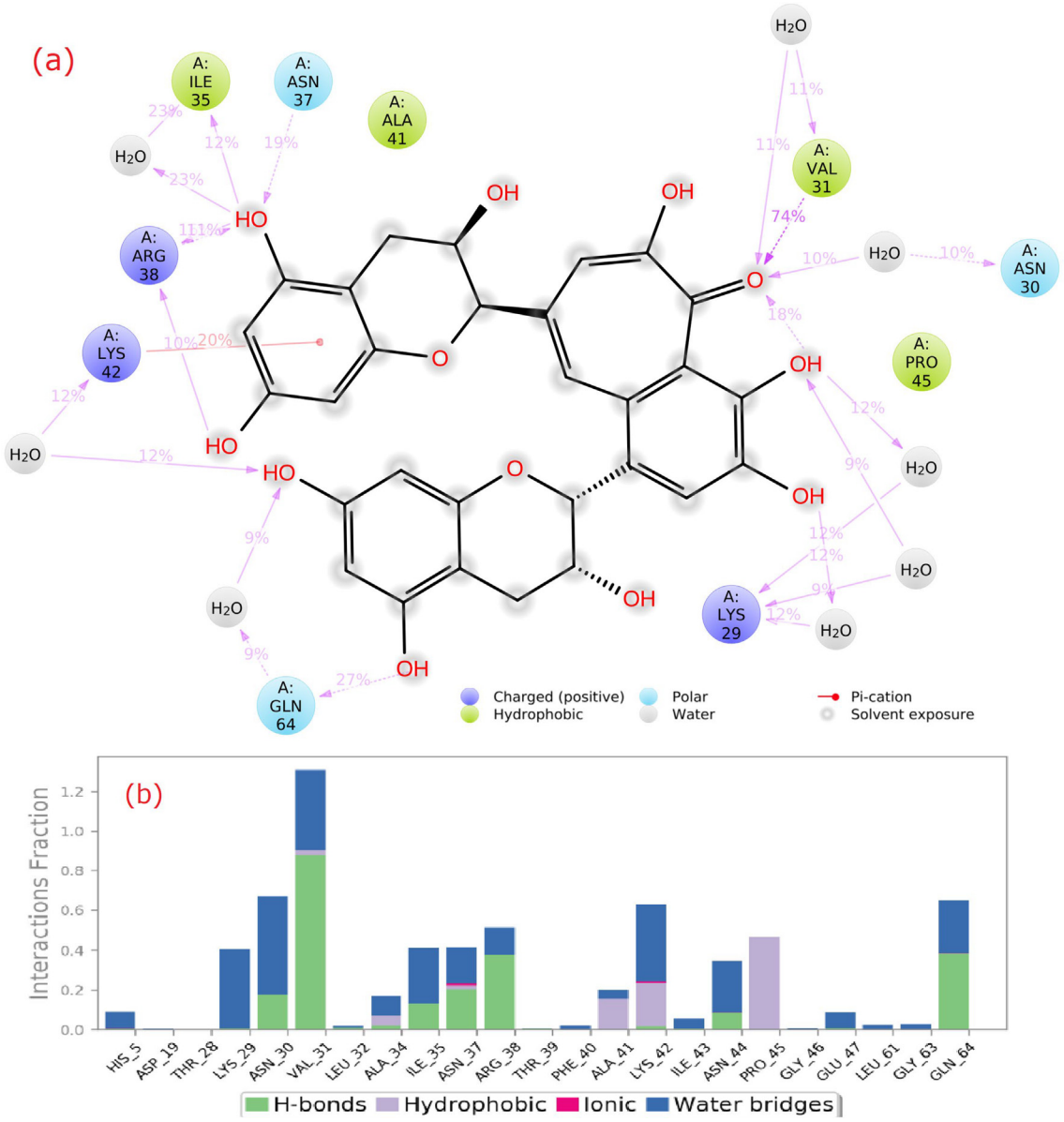

Fig. 8. Interactions and contact histograms of 4QWO residues during MD simulation.

absorption estimates the proportion of a medicine absorbed by the human gastrointestinal tract, which is frequently the primary drug absorption route, and absorption of less than 30% of the drug is considered poor. P-glycoprotein acts as a biological barrier that extrudes poisons and xenobiotics from cells. The antimicrobial peptides assessed in the study do not block P-glycoprotein I and II. In addition, the likelihood that a specific substance would dermally pass could be anticipated. If the log Kp of a chemical is no more than 2.5, it is considered less skin-permeable. It follows that the development of transdermal medication delivery might be of interest for cyclopeptides. LD_{50} is a common indicator of acute toxicity, and drug-induced liver damage is a major cause of drug attrition and a critical safety concern. Hepatotoxicity is linked to the disruption of normal liver function, and the predicted values of all cyclopeptides were positive. However, the expected values of skin sensitivity were negative.

5. QSAR studies

The activity, reactivity, and properties of test elements can be precisely predicted by QSAR analysis. The HyperChem Professional 8.0.3 application was used for the analysis. To reduce energy, an (MM +) force field, semi-empirical PM3 methods, and the Fletcher–Reeves conjugate gradient algorithm were used to optimise the ligand structures. Compound 5 had the highest partition coefficient (log P) of 8.48. Log P is extremely important to explain the biological activity of the generated compound. Log P is particularly crucial for determining the permeability of the cell membrane to medication.[40] Several crucial physical parameters such as the surface area, mass, volume, hydration energy, polarisability, refractivity, total energy, free energy, and RMS gradient were determined (Table 4) to propose ligand action.

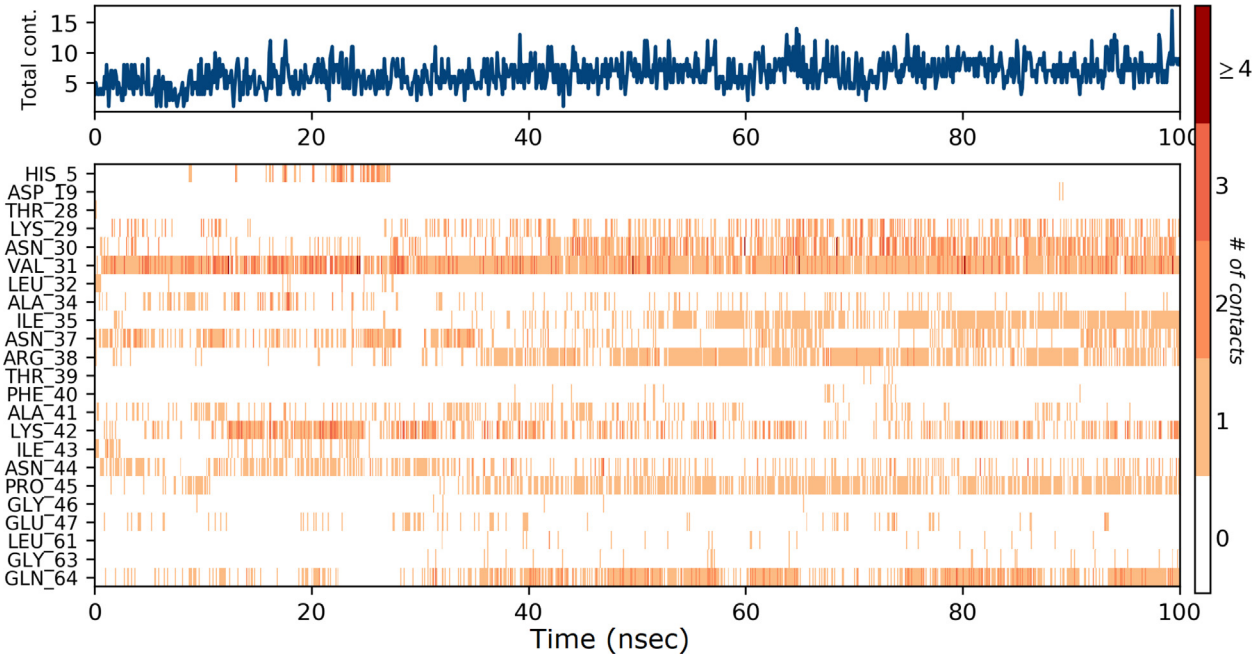

Fig. 9. P-L contact plots for the theaflavin–4QWO complex during MD simulation.

Table 3
ADMET properties of the ligands.

Property	Model Name	Predicted values					Decision unit
		Cidofovir (PubChem CID60613)	Rutin trihydrate (PubChem CID16218542)	Tecovirimat (PubChem CID 16124688)	Theaflavin (PubChem CID135403798)	Brincidofovir (PubChem CID483477)	
Absorption	Water solubility	−2.953	−2.931	−4.411	−2.892	−4.712	Numeric (log mol/L)
	$CaCO_2$ permeability	0.168	−1.115	1.064	−0.602	−0.419	Numeric (log Papp in 10^{-6} cm/s)
	Intestinal absorption (human)	51.766	12	95.401	58.515	68.212	Numeric (% Absorbed)
	Skin Permeability	−2.764	−2.735	−3.215	−2.735	−2.732	Numeric (log Kp)
	P-glycoprotein substrate	No	Yes	Yes	Yes	Yes	Categorical (Yes/No)
	P-glycoprotein I inhibitor	No	No	Yes	Yes	Yes	
	P-glycoprotein II inhibitor	No	No	No	Yes	Yes	
Distribution	VDss (human)	−0.516	0.062	0.252	0.064	−0.363	Numeric (log L/kg)
	Fraction unbound (human)	0.829	0.187	0.131	0.304	0.175	Numeric (Fu)
	BBB permeability	−1.491	−2.455	−0.261	−2.163	−2.234	Numeric (log BB)
	CNS permeability	−3.533	−5.853	−2.26	−4.039	−4.026	Numeric (log PS)
Metabolism	CYP2D6 substrate	No	No	No	No	No	Categorical (Yes/No)
	CYP3A4 substrate	No	No	Yes	No	Yes	
	CYP1A2 inhibitor	No	No	No	No	No	
	CYP2C19 inhibitor	No	No	Yes	No	No	
	CYP2C9 inhibitor	No	No	No	No	No	
	CYP2D6 inhibitor	No	No	No	No	No	
	CYP3A4 inhibitor	No	No	No	Yes	Yes	
Excretion	Total Clearance	−0.261	0.033	−0.49	0.225	0.912	Numeric (log ml/min/kg)
	Renal OCT2 substrate	No	No	No	No	No	Categorical (Yes/No)
Toxicity	AMES toxicity	No	Yes	No	No	No	
	Max. tolerated dose (human)	0.961	0.594	−0.531	0.437	0.74	Numeric (log mg/kg/day)
	hERG I inhibitor	No	No	No	No	No	Categorical (Yes/No)
	hERG II inhibitor	No	Yes	No	Yes	Yes	
	Oral Rat Acute Toxicity (LD50)	1.518	2.52	2.621	2.487	2.635	Numeric (mol/kg)
	Oral Rat Chronic Toxicity (LOAEL)	2.442	3.936	1.25	4.938	2.631	Numeric (log mg/kg_bw/day)
	Hepatotoxicity	Yes	No	No	No	Yes	Categorical (Yes/No)
	Skin Sensitisation	No	No	No	No	No	
	T. pyriformis toxicity	0.249	0.285	0.526	0.285	0.288	Numeric (log ug/L)
	Minnow toxicity	4.06	8.191	0.058	5.851	−0.588	Numeric (log mM)

Table 4
QSAR rating for optimised compounds.

Function parameter	Cidofovir (PubChem CID60613)	Rutin trihydrate (PubChem CID16218542)	Tecovirimat (PubChem CID 16124688)	Theaflavin (PubChem CID135403798)	Brincidofovir (PubChem CID483477)
Surface area (Appr) (Å^2)	427.94	583.22	433.08	545.77	1265.13
Surface area (Grid) (Å^2)	468.09	729.31	565.00	718.67	1098.94
Volume (Å^3)	757.89	1401.22	953.98	1338.67	1796.96
Hydration energy (kcal/mol)	−29.15	−46.76	−6.38	−44.31	−16.95
Log P	2.36	2.23	8.24	4.77	8.48
Refractivity (Å^3)	44.39	82.99	50.18	55.62	134.13
Polarizability (Å^3)	21.71	54.75	33.69	54.33	57.22
Mass (amu)	279.19	610.53	376.33	564.50	561.70
Total energy (kcal/mol)	−21.3922	31.9801	208.133	26.7081	3310.58
Dipole Moment (Debye)	0	0	0	0	0
Free energy (kcal/mol)	−21.3922	31.9801	208.133	26.7081	3310.58
RMS Gradient (kcal/Å mol)	0.07456	0.08764	0.08459	0.09366	0.08529

6. Significance of the study

In 2022, human mpox spread rapidly and caused a global health crisis. Although little is known about the virus's proteome, its genome has been extensively analysed and reported. An experimental mpox protein structure is yet to be reported excluding those obtained using computational models. Minasov et al. (2022) reported the first 1.52 Å resolution X-ray structure of the mpox protein A42R.[23] A42R, a cellular protein known to regulate actin cytoskeleton assembly, is structurally similar to profilins. Comparison of A42R with known profilin family members revealed critical structural differences supporting the earlier discovery that A42R did not bind to poly(L-proline) and only weakly bound to actin. The analysis suggested that A42R might discretely interact with phosphatidylinositol lipids. The data suggested that comparing cellular profilins might not readily determine the role of A42R in orthopoxvirus replication. This could facilitate the development of strategies to combat mpox should this infectious disease emerge as a pandemic in future. Continuously emerging and/or re-emerging deadly viruses such as SARS-CoV-2, Ebola, Marburg, and mpox prove that current antiviral regimens are insufficient.[44] Further, vaccine development is costly and time-consuming, and mass administration is even more challenging.[45,46] Moreover, vaccine development is impeded if a viral strain is highly evolving. This highlights the need to develop novel broad-spectrum antivirals with activity against an array of emerging viruses, as well as their mutants or variants. A42R profilin-like protein (PDB: 4QWO; small actin-binding protein involved in cell development, cytokinesis, membrane trafficking, and cell motility) from mpox virus Zaire-96-I-16 could be a target protein for designing the inhibitor. Anthracene structures closely related to mitoxantrone reportedly have the capacity to inhibit mpox and synergistically act with cidofovir.[47] Further, *in silico* and *in vitro* studies on stability could effectively improve the design of inhibitors in the future. One study suggested that glycocin F, a natural biomolecule, is effective against A42R profilin-like protein and has high potential as a broad-spectrum antiviral.[44] Analyses of the binding affinity of some curcumin derivatives against mpox and smallpox virus (PDB ID: 3IGC) demonstrated their outstanding ADMET characteristics.[48] Hence, these derivatives could also act as potential antiviral agents for mpox treatment.

Viral surface proteins could be promising candidates to develop vaccines. Thus, cysteine proteinase of mpox was selected as the target, and the primary amino acid sequence was analysed to develop suitable inhibitors.[49] N-(2-allylcarbamoyl-4-chlorophenyl) − 3,4-dimethoxy-benzamide exhibited the highest (−6.7 kcal/-mol) binding affinity against the core cysteine proteases of mpox.[50] Cefiderocol, dolutegravir, doxorubicin, and tipranavir bound strongly to both D9 decapping enzyme and TMPK of the Israeli mpox virus strain as target proteins in an *in silico* drug repurposing study [7,8].[51,52] Another study chose p37, topoisomerase 1, and thymidylate kinase as the primary targets because these are reportedly promising drug targets in treating other pox viruses.[53] Research to discover novel antivirals is necessary as zoonotic diseases increasingly threaten human life.

This work investigated the docking score, IC_{50}, ADMET properties, and QSAR data of several commonly used mpox drugs/mAbs (tecovirimat, brincidofovir, cidofovir) and bioactive phytochemicals (curcumin, rutin, and theaflavin). The results suggested that tecovirimat and theaflavin were the best binding ligands against PDB ID: 4QWO. The theaflavin–4QWO complex was further subjected to MD simulation as a novel drug lead. The complex had an impressive log P (4.77), validating its bioactivity. The test compounds passed all drug-likeness criteria, and thus, *in vitro* experimental validation of theaflavin and rutin might be considered to develop an effective drug against mpox.

7. Conclusion

This work investigated molecular docking of drugs/mAbs (tecovirimat, brincidofovir, cidofovir) prescribed against mpox to assess their affinity for A42R profilin-like protein. The compounds were compared against the phytochemicals curcumin, rutin, and theaflavin. A42R profilin-like protein from mpox virus (PDB ID: 4QWO) could represent a target for developing new lead compounds. Tecovirimat (−7.31 kcal/mol, IC_{50} = 4.39 μM) and theaflavin (−6.99 kcal/mol, IC_{50} = 7.54 μM) had the greatest affinity for the protein. The stability of the interactions of the theaflavin–4QWO complex was ascertained through MD simulation. The evaluated log P values for brincidofovir and tecovirimat obtained via QSAR analysis were greater than those of the other compounds. Theaflavin had an impressive log P of 4.77, which explained its biological activity. Per the ADMET data, the test compounds passed the drug-likeness criteria. These compounds might be considered for further *in vitro* experimental validation to develop economical and globally available anti-mpox drugs. This work should serve as a precursor to developing more effective therapeutic measures against mpox.

CRediT authorship contribution statement

Ranjan K. Mohapatra: Conceptualization, Supervision, Writing – original draft. **Ahmed Mahal:** Formal analysis, Writing – original draft. **Azaj Ansari:** Software, Visualization, Formal analysis, Writing – original draft. **Manjeet Kumar:** Software, Visualization, For-

mal analysis, Writing – original draft. **Jyoti Prakash Guru:** Formal analysis, Writing – original draft. **Ashish K. Sarangi:** Software, Visualization, Formal analysis, Writing – original draft. **Aly Abdou:** Software, Visualization, Formal analysis, Writing – original draft. **Snehasish Mishra:** Writing – review & editing. **Mohammed Aljeldah:** Formal analysis, Writing – original draft. **Bashayer M. AlShehail:** Formal analysis, Writing – original draft. **Mohammed Alissa:** Validation, Writing – original draft. **Mohammed Garout:** Validation, Writing – original draft. **Ahmed Alsayyah:** Validation, Writing – original draft. **Ahmad A. Alshehri:** Validation, Writing – original draft. **Ahmed Saif:** Validation, Writing – original draft. **Abdulaziz Alqahtani:** Validation, Writing – original draft. **Fahd A. Alshehri:** Validation, Writing – original draft. **Aref A. Alamri:** Validation, Writing – original draft. **Ali A. Rabaan:** Writing – review & editing.

Declaration of Competing Interest

The authors declare that they have no known competing financial interests or personal relationships that could have appeared to influence the work reported in this paper.

Acknowledgements

This study is supported via funding from Prince sattam bin Abdulaziz University project number (PSAU/2023/R/1445). We are thankful to our respective institutions for their support.

Appendix A. Supplementary material

Supplementary data to this article can be found online at https://doi.org/10.1016/j.jobb.2023.09.001.

References

1. CDC (2023), 2022 Mpox Outbreak Global Map, 02 Feb 2023. https://www.cdc.gov/poxvirus/monkeypox/response/2022/world-map.html (accessed on 03-02-2023).
2. Mohapatra RK, Tuli HS, Sarangi AK, et al. Unexpected sudden rise of human monkeypox cases in multiple non-endemic countries amid COVID-19 pandemic and salient counteracting strategies: another potential global threat? *Int J Surg*. 2022;103 106705.
3. Kozlov M. Monkeypox goes global: why scientists are on alert. *Nature*. 2022;606:15–16.
4. CDC, CDC and health partners responding to monkeypox case in the U.S., May 18, 2022. https://www.cdc.gov/media/releases/2022/s0518-monkeypox-case.html (accessed on 21-05-22).
5. Vallee A, Farfour E, Zucman D. Monkeypox virus: a novel sexually transmitted disease? A case report from France. *Trav Med Infect Dis.*. 2022;49 102394.
6. Rodriguez-Morales AJ, Amer FA. Monkeypox virus infection in women and non-binary people: uncommon or neglected? *Lancet*. 2022;400:1903–1905.
7. Mohapatra RK, Kandi V, Seidel V, et al. Monkeypox lineages amid the ongoing COVID-19 pandemic: a global public health concern. *Int J Surg*. 2022;107 106968.
8. Mohapatra RK, Mishra S, Kandi V, et al. Emerging monkeypox cases amid the ongoing COVID-19 pandemic in the Indian subcontinent: a probable healthcare challenge for South East Asia. *Front Public Health*. 2022;10 1066425.
9. Rizk JG, Lippi G, Henry BM, et al. Prevention and treatment of monkeypox. *Drugs*. 2022;82(9):957–963.
10. Chakraborty S, Chandran D, Mohapatra RK, et al. Clinical management, antiviral drugs and immunotherapeutics for treating monkeypox: an update on current knowledge and futuristic prospects. *Int J Surg*. 2022;105 106847.
11. Diaz JH. The disease ecology, epidemiology, clinical manifestations, management, prevention, and Control of increasing human infections with animal orthopoxviruses. *Wilderness Environ Med*. 2021;32(4):528–536.
12. Rodríguez-Cuadrado FJ, Pinto-Pulido EL, Fernandez-Parrado M. RF-potential treatments for monkeypox. *Actas Dermo-sifiliogr*. 2023;114:629–630.
13. Mohapatra RK, Mishra S, Rabaan AA, et al. Monkeypox breakthrough infections and side-effects: Clarion call for nex-gen novel vaccine. *New Microbe New Infect.*. 2023;52 101084.
14. Frisch M, Trucks GW, Schlegel HB, et al. Gaussian09, Revision d. 01, Gaussian. C, Wallingford CT 2009;201.
15. Frisch A, Nielson AB, Holder AJ. *GAUSSVIEW User Manual*. Pittsburgh, PA: GaussianInc; 2000.
16. Becke AD. Becke's three parameter hybridmethod using the LYP correlation functional. *J Chem Phys*. 1993;98:5648–5652.
17. Alghuwainem YAA, El-Lateef HMA, Khalaf MM, et al. Synthesis, DFT, Biological and Molecular Docking Analysis of Novel Manganese(II), Iron(III), Cobalt(II), Nickel(II), and Copper(II) Chelate Complexes Ligated by 1-(4-Nitrophenylazo)-2-naphthol. *Int J Mol Sci*. 2022;23(24):15614.
18. Arafath MA, Adam F, Ahamed MBK, et al. Ni(II), Pd(II) and Pt(II) complexes with SNO-group thiosemicarbazone and DMSO: Synthesis, characterization, DFT, molecular docking and cytotoxicity. *J Mol Struc.*. 2023;1278 134887.
19. Papajak E, Zheng J, Xu X, et al. Perspectives on basis sets beautiful: seasonal plantings of diffuse basis functions. *J Chem Theory Comput*. 2011;7:3027–3034.
20. Bajrai LH, Alharbi AS, El-Day MM, et al. Identification of Antiviral Compounds against Monkeypox Virus Profilin-like Protein A42R from Plantago lanceolata. *Molecules*. 2022;27:7718.
21. Mohapatra RK, Saikishore VP, Azam M, et al. Synthesis and physicochemical studies of a series of mixed ligand transition metal complexes and their molecular docking investigations against Coronavirus main protease. *Open Chem*. 2020;18:1495–1506.
22. Minasov G, Shuvalova L, Dubrovska I, et al. 1.52 Angstrom Crystal Structure of A42R Profilin-like Protein from Monkeypox Virus Zaire-96-I-16, Deposited: 2014-07-16, Released: 2014-08-06. PDB DOI: 10.2210/pdb4QWO/pdb. https://www.rcsb.org/structure/4qwo.
23. Minasov G, Inniss NL, Shuvalova L, et al. Structure of the Monkeypox virus profilin-like protein A42R reveals potential functional differences from cellular profilins. *Acta Crystallogr F Struct Biol Commun.*. 2022;78:371–377.
24. Pettersen EF, Goddard TD, Huang CC, et al. UCSF Chimera—A visualization system for exploratory research and analysis. *J Comput Chem*. 2004;25:1605–1612.
25. Morris GM, Huey R, Lindstrom W, et al. AutoDock4 and AutoDockTools4: automated docking with selective receptor flexibility. *J Comput Chem*. 2009;30 (16):2785–2791.
26. Morris GM, Goodsell DS, Halliday RS, et al. Automated docking using a Lamarckian genetic algorithm and an empirical binding free energy function. *J Comput Chem*. 1998;19:1639–1662.
27. Kaminski GA, Friesner RA, Tirado-Rives J, et al. Evaluation and parametrization of the OPLS-AA force field for proteins via comparison with accurate quantum chemical ncalucations on peptides. *J Phys Chem B*. 2001;105:6474–6487.
28. Jorgensen WL, Chandrasekhar J, Madura JD, et al. Comparison of simple potential functions for simulating liquid water. *J Chem Phys*. 1983;79:926–935.
29. Shinoda W, Mikami M. Rigid-body dynamics in the isothermal-isobaric ensemble: a test on the accuracy and computational efficiency. *J Comput Chem*. 2003;24(8):920–930.
30. Martyna GJ, Klein ML, Tuckerman M. Nose-Hoover chainsthe canonical ensemble via continuous dynamics. *J Chem Phys*. 1992;97:2635–2643.
31. Martyna GJ, Tobias DJ, Klein ML. Constant-pressure molecular dynamics algorithms. *J Chem Phys*. 1994;101:4177–4189.
32. Hrichi H, Elkanzi NAA, Ali AM, et al. A novel colorimetric chemosensor based on 2-[(carbamothioylhydrazono) methyl]phenyl 4-methylbenzenesulfonate (CHMPMBS) for the detection of Cu(II) in aqueous medium. *Res Chem Intermed*. 2023;49:2257–2276.
33. Shaaban S, Abdou A, Alhamzani AG, et al. Synthesis and in Silico Investigation of Organoselenium-Clubbed Schiff Bases as Potential Mpro Inhibitors for the SARS-CoV-2 Replication. *Life.*. 2023;13(4):912.
34. Domingo LR, Aurell MJ, Pérez P, Contreras R. Quantitative characterization of the local electrophilicity of organic molecules. *J Phys Chem. A*. 2002;106:6871–6875.
35. Jarad AJ, Dahi MA, Al-Noor TH, et al. Synthesis, spectral studies, DFT, biological evaluation, molecular docking and dyeing performance of 1-(4-((2-amino-5-methoxy) diazenyl) phenyl) ethanone complexes with some metallic ions. *J Mol Struct*. 2023;1287 135703.
36. Shokr EK, Kamel MS, Abdel-Ghany H, et al. Synthesis, characterization, and DFT study of linear and non-linear optical properties of some novel thieno[2,3-b] thiophene azo dye derivatives. *Mater Chem Phys*. 2022;290 126646.
37. Mohapatra PK, Chopdar KS, Dash GC, et al. In silico screening and covalent binding of phytochemicals of Ocimum sanctum against SARS-CoV-2 (COVID 19) main protease. *J Biomol Struct Dyn*. 2023;41:435–444.
38. Pant S, Singh M, Ravichandiran V, et al. Peptidelike and small-molecule inhibitors against Covid-19. *J Biomol Struct Dyn*. 2020;39(8):2904–2913.
39. Abdalla M, Mohapatra RK, Sarangi AK, et al. In silico studies on phytochemicals to combat the emerging COVID-19 infection. *J Saudi Chem Soc*. 2021;25 101367.
40. Mohapatra RK, Dhama K, El–Arabey AA, et al. Repurposing benzimidazole and benzothiazole derivatives as potential inhibitors of SARS-CoV-2: DFT, QSAR, molecular docking, molecular dynamics simulation, and in-silico pharmacokinetic and toxicity studies. *J King Saud Univ – Sci.*. 2021;33 101637.
41. Kumar S, Sharma PP, Shankar U, et al. Discovery of new hydroxyethylamine analogs against 3CLpro protein target of SARS-CoV-2: molecular docking, molecular dynamics simulation, and structure–activity relationship studies. *J Chem Inf Model*. 2020;60:5754–5770.
42. Jin Z, Wang Y, Yu X-F, et al. Structure-based virtual screening of influenza virus RNA polymerase inhibitors from natural compounds: Molecular dynamics simulation and MM-GBSA calculation. *Comput Biol Chem*. 2020;85 107241.
43. Guan L, Yang H, Cai Y, et al. ADMET-score – a comprehensive scoring function for evaluation of chemical drug- likeness. *Med Chem Commun.*. 2019;10:148–157.

44. Dassanayake MK, Khoo T-J, Chong CH, et al. Molecular docking and in-silico analysis of natural biomolecules against Dengue, Ebola, Zika, SARS-CoV-2 variants of concern and Monkeypox Virus. *Int J Mol Sci*. 2022;23:11131.
45. Mohapatra RK, Azam M, Mohapatra PK, et al. Computational studies on potential new anti-Covid-19 agents with a multi-target mode of action. *J King Saud Univ – Sci*.. 2022;34 102086.
46. Satapathy BS, Pattnaik G, Sahoo RN, et al. COVID-19 vaccines and their underbelly: Are we going the right way? *Health Sci Rep*. 2023.
47. Preet G, Oluwabusola ET, Milne BF, et al. Computational repurposing of mitoxantrone-related structures against Monkeypox Virus: a molecular docking and 3D pharmacophore study. *Int J Mol Sci*. 2022;23:14287.
48. Akash S, Hossain A, Hossain MS, et al. Anti-viral drug discovery against monkeypox and smallpox infection by natural curcumin derivatives: A Computational drug design approach. *Front Cell Infect Microbiol*. 2023;13 1157627.
49. Arasu MV, Vijayaragavan P, Purushothaman S, et al. Molecular docking of monkeypox (mpox) virus proteinase with FDA approved lead molecules. *J Infect Public Health*. 2023;16(5):784–791.
50. Bansal P, Gupta M, Sangwan S. Computational purposing phytochemicals against cysteine protease of Monkeypox virus: an in-silico approach. *J Pure Appl Microbiol*.. 2022;16(suppl 1):3144–3154.
51. Shah SSTH, Naeem I. In-silico targeting TMPK from monkey pox virus: Molecular docking analysis, density functional theory studies and molecular dynamic simulation analysis. *J Biomol Struct Dyn*. 2023. https://doi.org/10.1080/07391102.2023.2193998.
52. Sahoo AK, Augusthian PD, Muralitharan I, et al. In silico identification of potential inhibitors of vital monkeypox virus proteins from FDA approved drugs. *Mol Divers*. 2022. https://doi.org/10.1007/s11030-022-10550-1.
53. Srivastava V, Naik B, Godara P, et al. Identification of FDA-approved drugs with triple targeting mode of action for the treatment of monkeypox: a high throughput virtual screening study. *Mol Divers*. 2023. https://doi.org/10.1007/s11030-023-10636-4.